On the origin of multi-component bulk metallic glasses: Atomic size mismatches and de-mixing

Kai Zhang,[1,2] Bradley Dice,[2,3] Yanhui Liu,[1,2] Jan Schroers,[1,2] Mark D. Shattuck,[1,4] and Corey S. O'Hern[1,2,5,6]
[1]*Department of Mechanical Engineering and Materials Science, Yale University, New Haven, Connecticut 06520, USA*
[2]*Center for Research on Interface Structures and Phenomena, Yale University, New Haven, Connecticut 06520, USA*
[3]*William Jewell College, Liberty, Missouri 64068, USA*
[4]*Department of Physics and Benjamin Levich Institute, The City College of the City University of New York, New York, New York 10031, USA*
[5]*Department of Physics, Yale University, New Haven, Connecticut 06520, USA*
[6]*Department of Applied Physics, Yale University, New Haven, Connecticut 06520, USA*

(Received 25 May 2015; accepted 7 July 2015; published online 3 August 2015)

The likelihood that an undercooled liquid vitrifies or crystallizes depends on the cooling rate $\mathcal{R}$. The critical cooling rate $\mathcal{R}_c$, below which the liquid crystallizes upon cooling, characterizes the glass-forming ability (GFA) of the system. While pure metals are typically poor glass formers with $\mathcal{R}_c > 10^{12}$ K/s, specific multi-component alloys can form bulk metallic glasses (BMGs) even at cooling rates below $\mathcal{R} \sim 1$ K/s. Conventional wisdom asserts that metal alloys with three or more components are better glass formers (with smaller $\mathcal{R}_c$) than binary alloys. However, there is currently no theoretical framework that provides quantitative predictions for $\mathcal{R}_c$ for multi-component alloys. In this manuscript, we perform simulations of ternary hard-sphere systems, which have been shown to be accurate models for the glass-forming ability of BMGs, to understand the roles of geometric frustration and demixing in determining $\mathcal{R}_c$. Specifically, we compress ternary hard sphere mixtures into jammed packings and measure the critical compression rate, below which the system crystallizes, as a function of the diameter ratios σ_B/σ_A and σ_C/σ_A and number fractions x_A, x_B, and x_C. We find two distinct regimes for the GFA in parameter space for ternary hard spheres. When the diameter ratios are close to 1, such that the largest (A) and smallest (C) species are well-mixed, the GFA of ternary systems is no better than that of the optimal binary glass former. However, when $\sigma_C/\sigma_A \lesssim 0.8$ is below the demixing threshold for binary systems, adding a third component B with $\sigma_C < \sigma_B < \sigma_A$ increases the GFA of the system by preventing demixing of A and C. Analysis of the available data from experimental studies indicates that most ternary BMGs are below the binary demixing threshold with $\sigma_C/\sigma_A < 0.8$. © *2015 AIP Publishing LLC.* [http://dx.doi.org/10.1063/1.4927560]

I. INTRODUCTION

When atomic and molecular liquids are cooled sufficiently rapidly (i.e., above the critical cooling rate $\mathcal{R}_c$), they bypass crystallization and become trapped in disordered glassy configurations.[1] Avoiding crystallization in pure metals is very challenging and has only been achieved in experiments recently.[2] On the other hand, multi-component liquid alloys can form bulk metallic glasses (BMGs) that possess centimeter or greater casting thicknesses and critical cooling rates $\mathcal{R}_c < 1$ K/s.[3–5] BMGs have shown great promise as structural materials because they are amorphous with few defects and possess higher processability than crystalline metals.[6,7]

The conventional wisdom in the BMG research community is that BMGs should contain three or more atomic species[8] with atomic size differences above 12% (i.e., the ratio of the diameters of the smallest to the largest species should be $\lesssim$0.89).[9] Intuitively, more atomic components with different sizes introduce geometric frustration or "confusion," which delays crystallization.[4,10,11] Also, it has been suggested that a mixture of multiple atomic species leads to dense packing in the liquid state and thus enhanced stability of the glass.[11] The minimum critical cooling rate observed for binary BMGs is $\mathcal{R}_c \sim 10^2$ K/s, while it decreases to 10^{-1} and 10^{-2} K/s for ternary and quaternary systems, respectively. Alloys with similarly sized atomic constituents can only be casted into glassy thin films (see Table I in Appendix A). Even with these empirical rules, there is an enormous parameter space of potential BMGs and we lack a complete theoretical framework that would enable the prediction of $\mathcal{R}_c$ for each alloy in the design space.

A number of recent studies of hard-sphere mixtures have emphasized that dense atomic packing plays an important role in determining the structural properties and glassy dynamics of metallic alloys.[12–17] For example, the efficient cluster packing model has been successful at predicting spatial correlations in bulk metallic glasses.[13,14,17] In our prior work,[18] we directly measured the glass-forming ability (GFA) of binary hard-sphere systems to understand the competition between crystallization and glass formation. We found that binary metal-metal

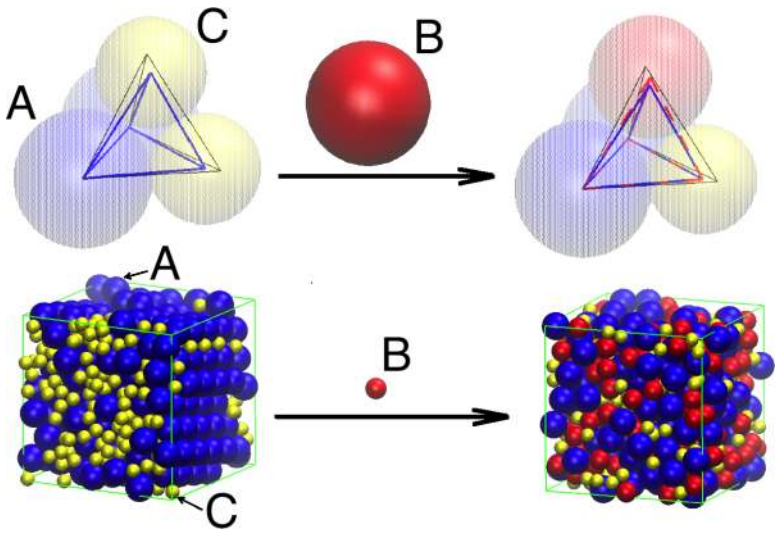

FIG. 1. (top) Comparison of the volumes of tetrahedral cells formed by the centers of face-centered cubic packed atoms with (left) two versus (right) three different sizes (i.e., either $\sigma_C/\sigma_A = 0.8$ with $x_B = 0$ or $\sigma_B/\sigma_A = 0.9$, $\sigma_C/\sigma_A = 0.8$, and $x_B > 0$). The tetrahedral volume for four same-sized atoms is 0.118 σ_A^3 (thin black line), while it is 0.084 σ_A^3 for two large and two small atoms (thick blue solid line) and 0.092 σ_A^3 for one small, one intermediate, and two large sized atoms (red dashed line). Thus, the distortion of the tetrahedral cell is smaller for the ternary system. (bottom) When atoms of an intermediate size ($\sigma_B/\sigma_A = 0.75$) are added to a binary system (with diameter ratio $\sigma_C/\sigma_A = 0.5$), it becomes more uniformly mixed and less ordered, i.e., with global bond orientational order parameter $Q_6 = 0.02$ (right) compared to 0.15 (left).

(i.e., transition metal-transition metal) BMGs, such as Cu–Zr, Cu–Hf, and Ca–Al, possess atomic size ratios $\alpha = \sigma_B/\sigma_A$ and small particle compositions x_B that occur in the region of parameter space with the smallest $\mathcal{R}_c$ for binary hard spheres.[18]

Can hard sphere models accurately capture the dependence of the GFA on the atomic size ratios and compositions for *multi-component* alloys? In this manuscript, we directly measure the glass-forming ability of ternary hard-sphere mixtures. We find two key results: (1) when the sizes of the three components are comparable, ternary systems behave similar to binary systems, and the GFA cannot be larger than that of a binary system consisting of the largest and smallest components. In this case, the packing efficiency of the ternary system is close to that of the binary systems (see Fig. 1 (top)). (2) When the diameter ratio of the smallest to the largest component is beyond the demixing limit ($\alpha \lesssim 0.8$[18]), adding a third component with an intermediate size can increase the GFA by preventing demixing. In this scenario, the packing fraction of the ternary system is significantly higher than the demixed binary system (see Fig. 1 (bottom)). This demixing mechanism has also been found in studies of segregation of granular media and other particulate solids.[19]

II. METHODS

We performed event-driven molecular dynamics simulations of $N = 500$ ternary hard spheres with diameters $\sigma_A \geq \sigma_B \geq \sigma_C$, number fractions $x_A = N_A/N$, $x_B = N_B/N$, and $x_C = N_C/N$, and the same mass m. We compressed systems initially prepared in liquid states at packing fraction $\phi = 0.25$ so that they exponentially approach static jammed packings at $\phi = \phi_J$ as a function of time. In particular, we first run the simulations at constant volume for a time interval τ and then compress the system instantaneously until the closest pair of spheres comes into contact.[15,18] This compression protocol is repeated until the reduced pressure (or compressibility factor) increases to 10^3, which corresponds to $(\phi_J - \phi)/\phi_J < 10^{-3}$. We vary the compression rate $R \equiv 1/\tau$ over 5 orders of magnitude.[18] Note that R is given in units of $\sqrt{k_B T/m\sigma_A^2}$ and $R = 1$ corresponds to a cooling rate $\mathcal{R} \approx 10^{12}$ K/s for metal alloys.[20] The crystal structures that compete with glass formation possess face-centered cubic (FCC)-like order, and thus, we characterize the positional order of the packings using the global bond orientational order parameter Q_6[21] averaged over 96 independent compression runs. The critical compression rate R_c is determined by the intersection of the mean and median Q_6 as a function of R (see Appendix B). To explore the glass-forming ability diagram for ternary systems, we studied more than 20 compositions and 10 pairs of atomic size ratios σ_B/σ_A and σ_C/σ_A. Additional details of the simulation methods can be found in Ref. 18.

III. RESULTS

In our previous studies of binary hard-sphere mixtures with diameter ratio $\alpha = \sigma_B/\sigma_A$ and small particle number fraction x_B, we found that the critical compression rate R_c decreases exponentially, $R_c \sim \exp[C(x_B)(1-\alpha)^3]$, where C is a composition-dependent constant, for $\alpha \gtrsim 0.8$ above the demixing limit (see Fig. 2). In contrast, for $\alpha \lesssim 0.8$, the large and small particles in binary systems can demix, which then induces crystallization. Thus, the glass-forming ability for binary hard-sphere systems first increases with decreasing α, but then begins to decrease for $\alpha \lesssim 0.8$.[18]

We first focus on ternary hard-sphere systems with weak size disparities. In Fig. 3 (top), we plot the critical compression rate R_c as a function of the number fractions of the three components x_A, x_B, and x_C at fixed diameter ratios $\sigma_B/\sigma_A = 0.95$ and $\sigma_C/\sigma_A = 0.9$. We find that the best glass-forming regime (i.e., the region with the smallest R_c) occurs on the binary composition line $\overline{AC}$ near $x_C = 1 - x_A \approx 0.6$ and $x_B = 0$. Adding the third component B with an intermediate size $\sigma_C < \sigma_B < \sigma_A$ causes a decrease in the glass-forming ability (or increase in R_c).

Recent studies have shown that phase-separated Barlow packings are the densest structures for binary hard spheres with diameter ratio $\alpha \gtrsim 0.66$.[22,23] However, we find that these packings are not kinetically accessible during compression for $\alpha \gtrsim 0.8$.[18] Instead, we find that the competing crystal for bidisperse hard-sphere systems in this diameter ratio regime is

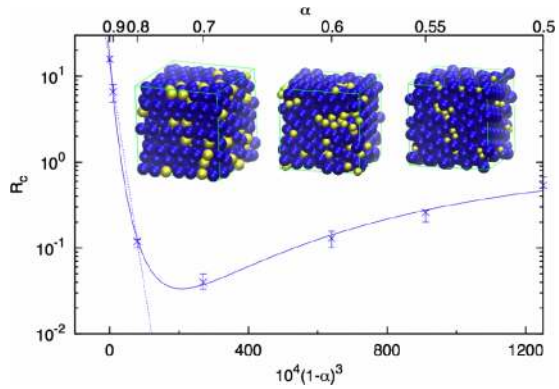

FIG. 2. In binary hard-sphere mixtures with diameter ratio $\alpha > \alpha_c(x_B)$ and fixed number fraction x_B of small particles, $\log_{10}R_c$ drops linearly with $(1-\alpha)^3$ (dotted line). For $\alpha < \alpha_c$, the large and small particles demix and R_c begins to increase with decreasing α. The composition-dependent threshold is $\alpha_c \approx 0.8$ for $x_B = 0.2$. The inset shows snapshots of configurations at $R \sim R_c$ for $x_B = 0.2$ and $\alpha = 0.9$, 0.7, and 0.5 from left to right, which illustrates increasing demixing as α decreases.

a deformed FCC crystal.[18] As shown in Fig. 1 (top), adding a third component with an intermediate size to a binary system in this diameter ratio regime reduces the FCC lattice distortion *as well as* the glass-forming ability. These results are consistent with experimental observations for bulk metallic glasses, which are summarized in Table I in Appendix A. There are no observed ternary bulk metallic glasses with weak size polydispersity, i.e., the diameter ratio of the smallest to the largest component satisfies $\alpha \gtrsim 0.8$.

We now consider ternary hard-sphere systems with a diameter ratio disparity that is beyond the demixing threshold, i.e., $\sigma_C/\sigma_A \lesssim 0.8$. In Fig. 3 (middle), we plot the critical compression rate R_c as a function of the compositions x_A, x_B, and x_C for ternary systems with diameter ratios $\sigma_B/\sigma_A = 0.95$ and $\sigma_C/\sigma_A = 0.5$. For this system, the smallest value of R_c does not occur at $x_B = 0$. Instead, for this ternary system, $R_c(x_B)$ possesses a minimum near $x_B \approx 0.4$ (see Fig. 3 (bottom)).

We can also measure the glass-forming ability at fixed composition and vary the diameters of one of the particles. In Fig. 4, we fix the compositions $x_A = x_B = x_C = 1/3$ and diameters σ_A and σ_C of two components and measure R_c as a function of the diameter ratio σ_B/σ_A. Note that, when $\sigma_B = \sigma_A$ (σ_C), the ternary systems reduce to binary systems with $x_C = 1/3$ (2/3). In experimentally observed ternary BMGs, when the diameters of two of the three components are similar, for instance, CuNi and AlTi, the ternary glass-forming ability diagram is symmetric and equivalent to that of the corresponding binary system.[24] We first focus on ternary systems with $\sigma_C/\sigma_A = 0.9$, which does not lead to demixing. When $\sigma_C/\sigma_A < \sigma_B/\sigma_A < 1$, R_c has a maximum at $\sigma_B/\sigma_A < 1$ and the ternary systems are worse glass formers than binary systems with $\sigma_B = \sigma_C$. These ternary systems show enhanced glass-forming ability above that for binary systems only when $\sigma_B/\sigma_A \lesssim 0.9$ (see Fig. 4).

In Fig. 4, we also consider fixed diameter ratio $\sigma_C/\sigma_A = 0.5$ for which the two components tend to demix. In this case, R_c does not possess a maximum at $\sigma_B/\sigma_A < 1$, and thus, these ternary systems can possess enhanced glass-forming ability compared to corresponding binary systems. The intro-

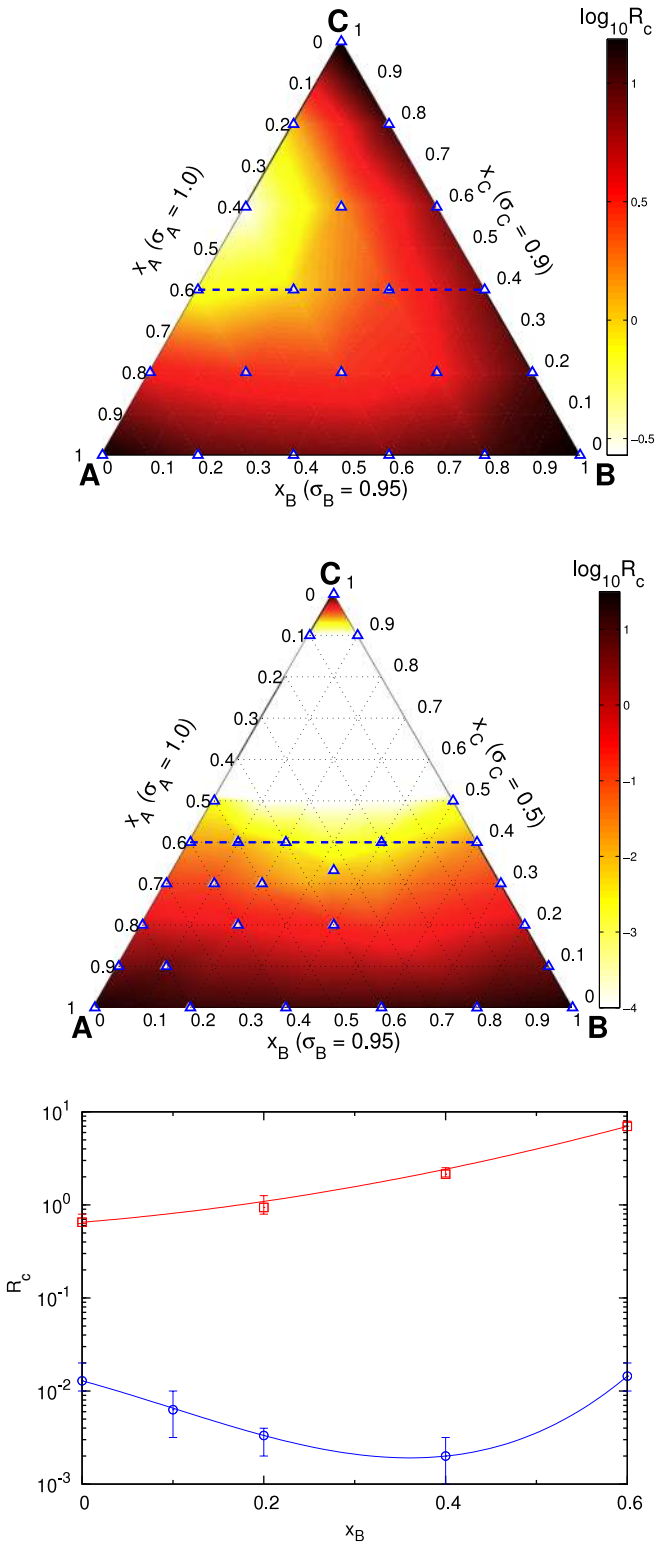

FIG. 3. (top) Critical compression rate R_c as a function of the compositions x_A, x_B, and x_C in ternary hard-sphere systems with diameter ratios $\sigma_B/\sigma_A = 0.95$ and $\sigma_C/\sigma_A = 0.9$. The minimum R_c occurs on the edge $\overline{AC}$, i.e., binary systems with $x_B = 0$. Moving perpendicular to $\overline{AC}$ on the diagram causes increases in R_c. (middle) Same as the top plot, but with diameter ratios $\sigma_B/\sigma_A = 0.95$ and $\sigma_C/\sigma_A = 0.5$. The minimum R_c no longer occurs for binary systems on the edge $\overline{AC}$. Note that the contour plots of $\log_{10}R_c$ are interpolated from ~20 simulation runs (triangles) and given on a color scale that decreases from dark to light. (bottom) R_c as a function of x_B at fixed $x_C = 0.4$ (dashed line in top and middle panels) for the diameter ratios studied in the top (squares) and middle (circles) panels.

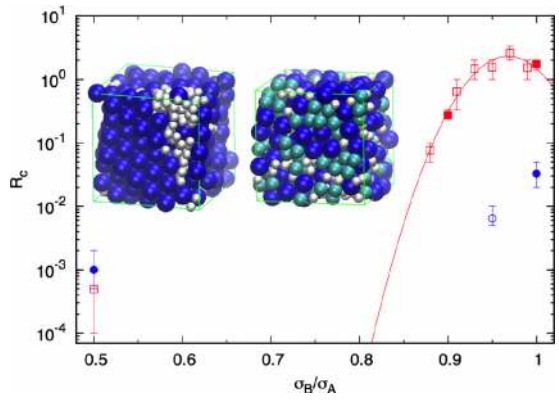

FIG. 4. The critical compression rate R_c as a function of the diameter ratio σ_B/σ_A at fixed composition $x_A = x_B = x_C = 1/3$ and $\sigma_C/\sigma_A = 0.9$ (squares) or $\sigma_C/\sigma_A = 0.5$ (circles). The solid line gives a polynomial fit to the data for $\sigma_C/\sigma_A = 0.9$ to show the qualitative trend. Ternary systems reduce to binary systems when $\sigma_B = \sigma_A$ or σ_C (solid symbols). In the inset, we show configurations obtained at a slow compression rate $R = 10^{-3}$ for $\sigma_B/\sigma_A = 0.5$ (left) and 0.75 (right). Large, intermediate, and small particles are shaded from dark to light.

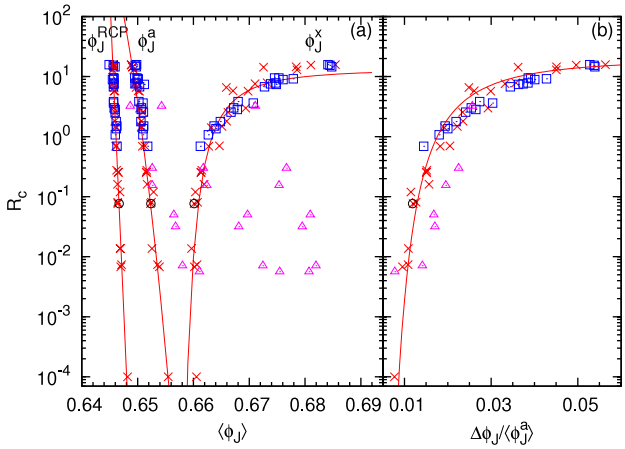

FIG. 5. (a) For each binary and ternary system, we plot the corresponding critical compression rate R_c and three definitions of the packing fraction at jamming: ϕ_J^{RCP} obtained in the $R \to \infty$ limit, ϕ_J^a for amorphous packings obtained at $R \sim R_c$, and ϕ_J^x for partially crystalline packings obtained at $R \sim R_c$ with $\phi_J^{RCP} < \phi_J^a < \phi_J^x$. The solid lines give polynomial fits to the data for the packing fraction at jamming for $\alpha \geq 0.8$. (b) R_c plotted versus the normalized difference $\Delta\phi_J/\langle\phi_J^a\rangle$, where $\Delta\phi_J = \phi_J^x - \phi_J^a$. The master curve (solid line) obeys $\log_{10} R_c \sim (\Delta\phi_J/\langle\phi_J^a\rangle)^{-2}$.[18] In (a) and (b), we considered binary systems with diameter ratios $\alpha \geq 0.8$ (crosses) and ternary systems with diameter ratio pairs $\sigma_B/\sigma_A = 0.95$ and $\sigma_C/\sigma_A = 0.9$, $\sigma_B/\sigma_A = 0.9$ and $\sigma_C/\sigma_A = 0.88$, and $\sigma_B/\sigma_A = 0.95$ and $\sigma_C/\sigma_A = 0.5$ (squares, circles, and triangles, respectively). In the absence of demixing, R_c versus the jammed packing fraction for ternary systems is quantitatively similar to that for binary systems. However, ternary systems that demix deviate from the master curve.

duction of the third component with an intermediate size σ_B prevents demixing. As shown in the insets of Fig. 4, binary systems with $\sigma_B/\sigma_A = 0.5$ demix and crystallize (left), while ternary systems with $\sigma_B/\sigma_A = 0.75$ remain well-mixed and amorphous (right). Although the large particles A exclude the small ones C, A particles mix with B particles and B particles mix with C particles, which leads to effective mixing of A and C particles.

Because packing efficiency and vibrational entropy determine the stability of crystals in hard-sphere systems,[25,26] one can correlate the packing fraction at jamming ϕ_J with the critical compression rate R_c as demonstrated in binary systems.[18] We study three relevant packing fractions: ϕ_J^{RCP} obtained in the limit $R \to \infty$,[27–29] ϕ_J^a for amorphous packings obtained at $R \sim R_c$, and ϕ_J^x for partially crystalline packings obtained at $R \sim R_c$.

We do not correlate the critical cooling rate with the packing fraction of the densest crystalline packing for a given set of particle number fractions and diameter ratios.[22,23,30,31] We have shown in previous work[18] and confirmed here that the crystalline configurations that compete with glass formation for compression rates $R \sim R_c$ are not the densest ones. For $\alpha \gtrsim 0.8$, the crystalline configurations that compete with glass formation are polycrystalline FCC solid solutions, not the denser phase-separated Barlow-packed crystals of small and large particles. For all $\alpha \lesssim 0.8$, the crystalline configurations that compete with glass formation are partially demixed Barlow-packed crystals, not compound crystal structures. We find little correlation between the packing fraction of the densest crystalline structures and the critical compression rate of the system.

As shown in Fig. 5 for ternary systems with diameter ratio pairs $\sigma_B/\sigma_A = 0.95$ and $\sigma_C/\sigma_A = 0.9$ and $\sigma_B/\sigma_A = 0.9$ and $\sigma_C/\sigma_A = 0.88$ that do not demix, the relations between R_c and packing fraction ϕ_J at jamming follow the trends for binary systems, i.e., as ϕ_J^a and ϕ_J^x approach each other, $R_c \to 0$. In addition, the packing fraction in these ternary systems is not larger than in binary systems, contrary to the intuition that ternary systems are always denser than binary systems and thus possess higher glass-forming abilities.[11] These results show that ternary systems with weak diameter ratio disparities can be described effectively as binary systems since the additional intermediate-sized particles only decrease the particle size gradient in the original binary system without changing the mechanism that drives crystallization.[18,32] The deviations from the master curve (solid lines) in Fig. 5 indicate demixing in the ternary system with diameter ratio pairs $\sigma_B/\sigma_A = 0.95$ and $\sigma_C/\sigma_A = 0.5$. However, compared with the binary system with diameter ratio $\alpha = 0.5$,[18] the deviation of the ternary system from the master curve is smaller, which indicates weaker demixing than the binary system. The packing fractions for all of the systems in Fig. 5 were also studied as a function of system size. The packing fractions ϕ_J^{RCP}, ϕ_J^a, and ϕ_J^x obtained in the large-system limit differ from those presented in Fig. 5 by less than 1%, which is consistent with our prior results.[33]

In Fig. 6, we illustrate the diameter ratio variation for 15 180 combinations of three elements from a set of 46 potential BMG-forming elements. The atomic sizes of the elements are given by their metallic radii,[12,13] which are shown in the inset of Fig. 6. We define the component types so that they satisfy $\sigma_C \leq \sigma_B \leq \sigma_A$, and thus, the data occur in left corner of the plot.

In previous studies, we predicted that the optimal binary hard-sphere glass formers occur in the diameter ratio range $0.73 < \alpha < 0.82$, where α is sufficiently small to prevent ordering, but not too small to cause demixing. We can estimate the optimal glass-forming regime in the σ_B/σ_A and σ_C/σ_A plane for ternary systems using the following arguments. First,

two of the boundaries ($\overline{ab}$ and $\overline{cd}$) can be obtained directly from the results for binary systems. Because adding a third intermediate-sized component can prevent demixing of the original two components, we expect that the lower bound for the diameter ratio in ternary BMG-forming systems to be much smaller than 0.73. We propose that 0.73^2 is the lower bound for the diameter ratio for ternary systems. In this case, $\sigma_C/\sigma_A = 0.73^2$, $\sigma_B/\sigma_A = 0.73$, and $\sigma_C/\sigma_B = 0.73$ (point *e* in Fig. 6), and thus, all binary combinations are above the lower bound of the good GFA regime.

We predict that good BMG-forming alloys will occur within the polygon defined by lines connecting the points (a)-(e) in the σ_B/σ_A and σ_C/σ_A parameter space. 33 ternary alloy systems have been observed experimentally in amorphous states (filled circles),[5,13,34] all of which fall in the good glass-forming regime predicted by hard-sphere systems. For the experimentally observed ternary BMGs, the diameter ratio for the smallest versus the largest particle σ_C/σ_A satisfies $\alpha < 0.8$, which is below the demixing limit for binary systems. Therefore, the experimentally observed ternary BMGs have better GFA than the best binary glass-forming alloys. In addition, the experimentally observed BMGs tend to be positioned away from the boundaries $\overline{ab}$ and $\overline{cd}$. As ternary systems approach $\overline{ab}$ ($\overline{cd}$), $\sigma_B/\sigma_A \to 1$ ($\sigma_C/\sigma_A \to 1$), which causes them to behave as binary systems and reduces their glass-forming ability. The experimentally observed ternary BMGs cluster roughly into three groups: (i) (Zr,Hf,Sn,Mg)–(Al,Ti,Nb)–(Cu,Ni,Co), (ii) (Y,Ln)–Al–(Cu,Ni,Co), and (iii) (Au,Pd,Pt)–(Cu,Ni)–(Si,P) (see Table I in Appendix A).

IV. CONCLUSION

We performed event-driven molecular dynamics simulations of ternary hard-sphere systems over a wide range of compositions and diameter ratios to identify the optimal glass-forming parameter regime. We identify two mechanisms for optimizing the glass-forming ability in ternary systems. First, if the sizes of the three components are similar, i.e., less than 10% deviation in the diameters, the ternary system behaves effectively as a binary system containing only the largest and smallest particles. Second, if the diameter ratio of the smallest to the largest particle is below the demixing threshold $\sigma_C/\sigma_A \lesssim 0.8$, adding the third component *B* with $\sigma_C/\sigma_A < \sigma_B/\sigma_A < 1$ will dramatically enhance the glass-forming ability above that for binary systems. We show that all experimentally observed ternary BMGs to date possess atomic species for which the diameter ratio of the smallest to the largest satisfies $\sigma_C/\sigma_A < 0.8$. Thus, an efficient strategy to design BMGs with good GFA is to maintain large atomic size differences and prevent demixing by introducing three or more atomic components.

We recognize that the inter-atomic potentials describing BMGs are far more complicated than the pairwise additive hard-sphere potential that we employed. For example, the apparent distance between the repulsive cores of two elements can be shorter than the mean core size of the two elements.[35] Also, in a more exact treatment, Friedel oscillations originating from perturbations to the electron density should be included since they are known to change the stability of various crystalline lattices.[36] Despite these caveats and others, we show that the hard-sphere model is able to semi-quantitatively predict the regime of optimal glass-forming ability in experimentally observed ternary BMGs. In the near future, we will consider how non-additivity of the particle diameters, attractive interactions, and barriers in the pairwise potential and multi-body interactions affects crystal and glass formation and modifies the hard-sphere predictions.[37]

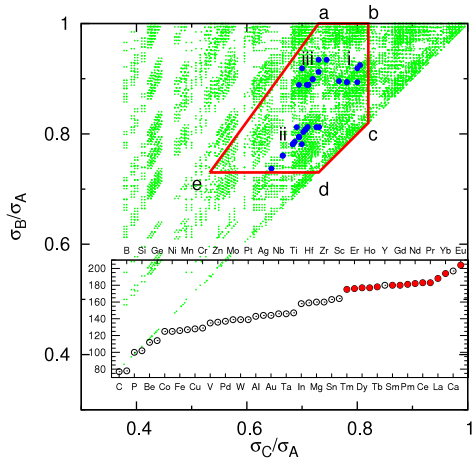

FIG. 6. Scatter plot of the diameter ratios σ_B/σ_A versus σ_C/σ_A with $\sigma_C \le \sigma_B \le \sigma_A$ for all 15 180 combinations of three elements chosen from 46 possible BMG-forming elements (dots). 33 of the combinations (filled circles) have been shown experimentally to form BMGs and occur in roughly three main clusters: (i) (Zr,Hf,Sn,Mg)–(Al,Ti,Nb)–(Cu,Ni,Co), (ii) (Y,Ln)–Al–(Cu,Ni,Co), and (iii) (Au,Pd,Pt)–(Cu,Ni)–(Si,P). The predicted BMG-forming alloys are located within the polygon bounded by the solid lines. The inset gives the atomic radii in pm of the 46 potential BMG-forming elements ordered from smallest to largest.[5,12,13] The symbols of the elements alternate from top to bottom on the horizontal axis and the lanthanide elements are shown as filled circles.

ACKNOWLEDGMENTS

The authors acknowledge primary financial support from the NSF MRSEC No. DMR-1119826 (K.Z. and B.D.) and partial support from NSF Grant Nos. DMR-1006537 (C.O.) and CBET-0968013 (M.S.). We also acknowledge support from the Kavli Institute for Theoretical Physics (through NSF Grant No. PHY-1125915), where some of this work was performed. This work also benefited from the facilities and staff of the Yale University Faculty of Arts and Sciences High Performance Computing Center and the NSF (Grant No. CNS-0821132) that in part funded acquisition of the computational facilities.

APPENDIX A: GLASS-FORMING ABILITY OF EXPERIMENTALLY OBSERVED BMGs

In this appendix, we provide a table of the critical cooling rates $\mathcal{R}_c$ in units of K/s for experimentally observed binary and ternary BMGs; see Table I. In the first column, we list each class of binary and ternary BMGs according to the atom types that are present. Atom types with similar sizes and properties are grouped together in parentheses. In the second column, we provide examples of specific alloys within each BMG class. The third column gives diameter ratios: σ_B/σ_A with $\sigma_B \le \sigma_A$

for binary systems and σ_B/σ_A and σ_C/σ_A with $\sigma_C \leq \sigma_B \leq \sigma_A$ for ternary systems.[5,12,13,34]

APPENDIX B: MEASUREMENT OF CRITICAL COMPRESSION RATE R_c IN SIMULATIONS

In this appendix, we describe the measurement of the critical compression rate R_c in the molecular dynamics simulations of hard-spheres. We performed 96 independent runs to generate jammed configurations at each compression rate R. We find that the distribution $P(Q_6)$ of the global bond orientational order parameter becomes bimodal as $R \to R_c$ with peaks that correspond to amorphous and partially crystalline configurations. In Fig. 7, we show that both the mean and median Q_6 possess a sigmoidal shape on a logarithmic scale in R. We define R_c as the critical compression rate at which the mean and median Q_6 intersect. A configuration is determined to be crystalline (amorphous) if $Q_6 > Q_c$ ($Q_6 < Q_c$), where Q_c is the value of Q_6 at which the mean and median Q_6 intersect. Since the distribution $P(Q_6)$ is bimodal at $R \approx R_c$, one can also fit $P(Q_6)$ by the sum of two Gaussian distributions and identify R_c as the rate at which the two Gaussian contributions have equal area. This method can be more time efficient since it avoids measurements at $R \ll R_c$.

TABLE I. Glass-forming ability (characterized by the critical cooling rate $\mathcal{R}_c$ in units of K/s) and atomic diameter ratio[a] for experimentally observed binary and ternary BMGs.[5,13,34] Elements with similar sizes and properties are grouped together using parentheses (see also Fig. 6). The lanthanide elements[b] are indicated by Ln.

Binary system	Alloy	$\mathcal{R}_c$ (K/s)	Diameter ratio σ_B/σ_A
Fe–B	$Fe_{91}B_9$	2.6×10^7	0.62
(Au,Pd)–Si			
	$Au_{80}Si_{20}$	1.0×10^6	0.71
	$Pd_{95}Si_5$	5.0×10^7	0.74
	$Pd_{82}Si_{18}$	1.8×10^3	
	$Pd_{75}Si_{25}$	1.0×10^6	
Ti–Be	$Ti_{63}Be_{37}$	6.3×10^6	0.76
Zr–Be	$Zr_{65}Be_{35}$	1.0×10^7	0.7
Zr–Cu	$Zr_{50}Cu_{50}$	250	0.8
Nb–Ni	$Nb_{40}Ni_{60}$	1400	0.85
Ternary system	**Alloy[c]**	$\mathcal{R}_c$ (K/s)	Diameter ratios $\sigma_C/\sigma_A, \sigma_B/\sigma_A$
Au–Si–Ge	$Au_{77.8}Si_{8.4}Ge_{13.8}$	3.0×10^6	0.71, 0.79
(Au,Pd,Pt)–(Cu,Ni)–(Si,P)			
	$Pd_{40}Ni_{40}P_{20}$	0.167	0.73, 0.91
	$Pd_{77}Cu_6Si_{17}$	125	0.74, 0.93
	$Pd_{79.5}Cu_4Si_{16.5}$	500	
	$Pd_{77.5}Cu_6Si_{16.5}$	100	
(Y,Ca,Ln)–Mg–(Cu,Ni)			
	$Nd_{15}Mg_{70}Ni_{15}$	178.2	0.69, 0.88
	$Nd_{15}Mg_{65}Ni_{20}$	30	
	$Nd_{10}Mg_{75}Ni_{15}$	46.1	
	$Nd_5Mg_{77}Ni_{18}$	49 000	
	$Nd_5Mg_{90}Ni_5$	53 000	
	$Nd_{10}Mg_{80}Ni_{10}$	1 251.4	
	$Y_{10}Mg_{65}Cu_{25}$	50	0.71, 0.89
	$Gd_{10}Mg_{65}Cu_{25}$	1	0.71, 0.89
(Y,Ln)–Al–(Cu,Ni,Co)			
	$La_{55}Al_{25}Ni_{20}$	67.5	0.66, 0.76
	$La_{55}Al_{25}Cu_{20}$	72.3	0.68, 0.76
	$La_{66}Al_{14}Cu_{20}$	37.5	
(Zr,Hf,Sn,Mg)–(Al,Ti,Nb)–(Cu,Ni,Co)			
	$Zr_{66}Al_8Ni_{26}$	66.6	0.78, 0.89
(Zn,Al,Ag)–Mg–Ca			
	$Zn_{20}Mg_{15}Ca_{65}$	20	0.69, 0.81

[a]Atomic radii are obtained from Refs. 12 and 13, which determine the atomic sizes using the first peak of the radial distribution function of amorphous liquid alloys or half of the spacing between atoms in metallic solids.

[b]Ln refers to the series of fifteen metallic elements (La, Ce, Pr, Nd, Pm, Sm, Eu, Gd, Tb, Dy, Ho, Er, Tm, Yb, and Lu) with atomic numbers 57-71. Together with two more chemically similar elements Sc and Y, these seventeen elements are collectively known as the rare earth elements and are typically the largest sized component in BMGs.

[c]For each system, we only list alloys for which the critical cooling rate $\mathcal{R}_c$ has been reported. Other alloys such as Ca–Mg–Cu, Hf–Al–Cu, and Y–Al–Co are also BMG formers, but with unreported values of $\mathcal{R}_c$.

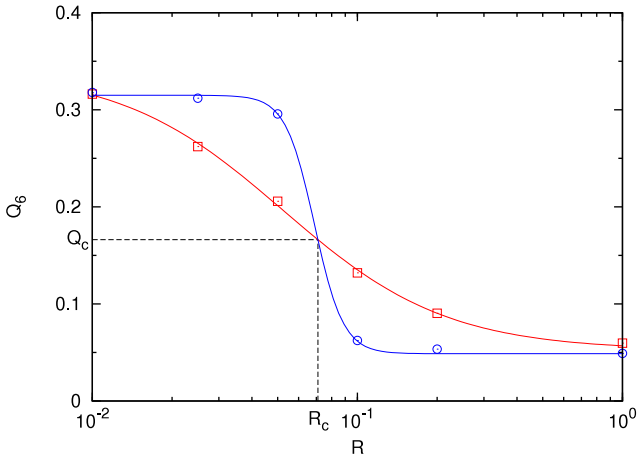

FIG. 7. The mean and median Q_6 as a function of compression rate R for ternary hard spheres with diameter ratios $\sigma_C/\sigma_A = 0.88$ and $\sigma_B/\sigma_A = 0.9$ and compositions $x_A = x_B = x_C = 1/3$. The critical compression rate R_c and bond orientational order parameter Q_c are defined by the intersection of the mean and median Q_6. The solid lines are fits to a logistic function.

[1]P. G. Debenedetti and F. H. Stillinger, Nature **410**, 259 (2001).
[2]L. Zhong, J. Wang, H. Sheng, Z. Zhang, and S. X. Mao, Nature **512**, 177 (2014).
[3]H. S. Chen, Rep. Prog. Phys. **43**, 353 (1980).
[4]A. L. Greer, Science **267**, 1947 (1995).
[5]A. Inoue, Acta Mater. **48**, 279 (2000).
[6]A. L. Greer and E. Ma, MRS Bull. **32**, 611 (2007).
[7]J. Schroers, Phys. Today **66**(2), 32 (2013).
[8]A. L. Greer, Mater. Today **12**, 14 (2009).
[9]A. Inoue, T. Zhang, and A. Takeuchi, Mater. Sci. Forum **269-272**, 855 (1998).
[10]A. L. Greer, Nature **366**, 303 (1993).
[11]T. Zhang, A. Inoue, and T. Masumoto, Mater. Trans. **32**, 1005 (1991).
[12]T. Egami and Y. Waseda, J. Non-Cryst. Solids **64**, 113 (1984).
[13]D. B. Miracle, W. S. Sanders, and O. N. Senkov, Philos. Mag. **83**, 2409 (2003).
[14]D. B. Miracle, Nat. Mater. **3**, 697 (2004).
[15]P. Jalali and M. Li, Intermetallics **12**, 1167 (2004).
[16]H. W. Sheng, W. K. Luo, F. M. Alamgier, J. M. Bai, and E. Ma, Nature **439**, 419 (2006).
[17]D. B. Miracle, Acta Mater. **61**, 3157 (2013).
[18]K. Zhang, W. W. Smith, M. Wang, Y. Liu, J. Schroers, M. D. Shattuck, and C. S. O'Hern, Phys. Rev. E **90**, 032311 (2014).
[19]J. L. Olsen and E. G. Rippie, J. Pharm. Sci. **53**, 147 (1964).
[20]T. M. Truskett, S. Torquato, and P. G. Debenedetti, Phys. Rev. E **62**, 993 (2000).
[21]P. J. Steinhardt, D. R. Nelson, and M. Ronchetti, Phys. Rev. B **28**, 784 (1983).
[22]A. B. Hopkins, Y. Jiao, F. H. Stillinger, and S. Torquato, Phy. Rev. Lett. **107**, 125501 (2011).
[23]A. B. Hopkins, F. H. Stillinger, and S. Torquato, Phys. Rev. E **85**, 021130 (2012).
[24]A. Takeuchi and A. Inoue, Mater. Trans. **42**, 1435 (2001).
[25]D. Turnbull and M. H. Cohen, J. Chem. Phys. **34**, 120 (1961).
[26]G. Parisi and F. Zamponi, Rev. Mod. Phys. **82**, 789 (2010).
[27]S. Torquato, T. M. Truskett, and P. G. Debenedetti, Phys. Rev. Lett. **84**, 2064 (2000).
[28]S. Torquato and F. H. Stillinger, Rev. Mod. Phys. **82**, 2633 (2010).
[29]A. B. Hopkins, F. H. Stillinger, and S. Torquato, Phys. Rev. E **88**, 022205 (2013).
[30]J. K. Kummerfeld, T. S. Hudson, and P. Harrowell, J. Phys. Chem. B **112**, 10773 (2008).
[31]T. Hudson and P. Harrowell, J. Phys. Chem. B **112**, 8139 (2008).
[32]Y. Li, Q. Guo, J. A. Kalb, and C. V. Thompson, Science **322**, 1816 (2008).
[33]C. F. Schreck, C. S. O'Hern, and L. E. Silbert, Phys. Rev. E **84**, 011305 (2011).
[34]Z. Long, H. Wei, Y. Ding, P. Zhang, G. Xie, and A. Inoue, J. Alloys Compd. **475**, 207 (2009).
[35]Y. Q. Cheng, E. Ma, and H. W. Sheng, Phys. Rev. Lett. **102**, 245501 (2009).
[36]J. P. K. Doye, D. J. Wales, F. H. M. Zetterling, and M. Dzugutov, J. Chem. Phys **118**, 2792 (2003).
[37]K. Zhang, M. Fan, Y. Liu, J. Schroers, M. D. Shattuck, and C. S. O'Hern, "The effects of core softness, non-additivity, medium-range repulsion, and many-body interactions on the glass-forming ability of bulk metallic glasses" (unpublished).